Structural analysis of the TPI-Manchester, a thermolabile variant of human triosephosphate isomerase

Jorge Miguel Romero*

Centro de Investigaciones en Química Biológica de Córdoba (CIQUIBIC, Universidad Nacional de Córdoba - Consejo Nacional de Investigaciones Científicas y Técnicas (UNC-CONICET)), Departamento de Química Biológica Ranwel Caputto, Facultad de Ciencias Químicas, Universidad Nacional de Córdoba, X5000HUA Córdoba, Argentina.

*Corresponding author
Centro de Investigaciones en Química Biológica de Córdoba (CIQUIBIC), Departamento de Química Biológica Ranwel Caputto, Facultad de Ciencias Químicas, UNC-CONICET, Haya de la Torre s/n, Pabellón Argentina Ala Oeste, X5000HUA Córdoba, Argentina. Tel.: +54-351-53538555; Fax: +54-351-4334074; E-mail: jorge.romero@unc.edu.ar

Keywords

Triosephosphate isomerase deficiency; X-ray crystallization; stability; flexibility

Abstract

Human triosephosphate isomerase G122R, also known as TPI-Manchester, is a thermolabile variant detected in a screening of more than 3,400 individuals from a population in Ann Arbor, Michigan. Here, the crystallographic structure of G122R was solved to determine the molecular basis of its thermal stability. Structural analysis revealed an increase in the flexibility of residues at the dimer interface, even though R122 is about 20 Å away, suggesting that long-range electrostatic interactions may play a key role in the mutation effect.

1. Introduction

Human triosephosphate isomerase (hTPI) is a homodimeric enzyme that catalyze the glycolytic conversion of dihydroxyacetone phosphate to glyceraldehyde-3-phosphate. The crystallographic structure revealed that each protomer adopts a (β/α) 8-barrel fold [1] (Fig. 1a). The (β/α) 8-barrel fold defines two faces located in the two mouths of the barrel. One of these faces is called the catalytic face because it contains the catalytic site [2] (Fig.

1b and c). On the noncatalytic face, there are six loops and one α-helix connecting the secondary elements of the (β/α) 8-barrel fold (Fig. 1d). On the catalytic face, the connections are more complex, involving two α-helixes and two larger loops (Fig. 1d). One of these loops is the dimeric loop, which is involved in the dimeric interface. It protrudes from the bulk of its own subunit and docks into a pocket of the other subunit. The other is a catalytic loop that adopts a closed/open conformation depending on substrate binding [3].

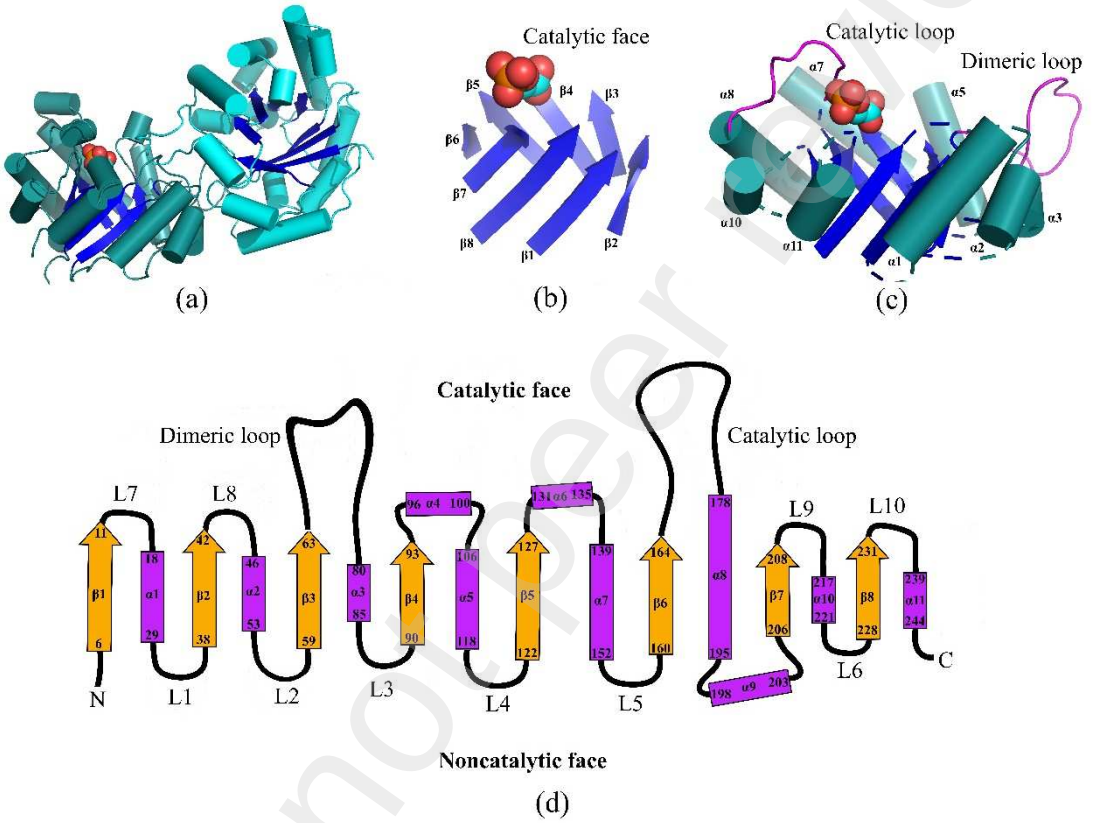

Figure 1: Structural description of hTPI (holo-wt). (a). Subunits A and B are shown in cyan and dark cyan, respectively. In both subunits the β-sheets are shown in blue. (b). The eight β-strands of the (β/α) 8-barrel fold of the B subunit. (c). The secondary structure elements of the B subunit belonging only to the (β/α) 8-barrel fold. (d). Topology diagram of hTPI. Orange arrows indicate β-strands, purple cylinders indicate helices, numbers included in the secondary structure elements indicate residues; loops are indicated by L. The substrate analogue 2-PG is shown in spheres (a, b and c).

Missense hTPI mutations affecting either enzymatic activity, dimer interface or thermostability have been described in individuals [4-8]. TPI deficiency results from being homozygous for some of these mutations or heterozygous between them. TPI deficiency belongs to a group of disorders known as glycolytic enzymopathies, which are characterised by chronic haemolytic anaemia, severe progressive neurological dysfunction such as cardiomyopathy, susceptibility to infections, etc. [4-7]. Crystallographic studies were performed to elucidate the structural basis of the disease in

the E104D mutant (the most lethal mutation) and the F240L mutant [9,10]. Both are thermolabile and the mutations affect non-covalent interactions at the dimeric interface. The G122R mutant, also known as TPI-Manchester, was described and studied by Dr. H.W. Mohrenweiser and was found to be thermolabile [11-13]. It was found in a heterozygous individual with a normal allele. To date, no patients with homozygous G122R or compound heterozygotes with another mutation have been reported. Therefore, it is not possible to assess the severity of the mutation. Here we have solved by X-ray the structure of hTPI-G122R in the presence (holo-G122R) or absence (apo-G122R) of the substrate analogue phosphoglycolic acid (2-PG). The aims of this study were: (a) to identify the region of the structure affected by the mutation by comparing the B'-factors between wt and mutant hTPI and to determine whether, as E104D and F240L, the dimeric interface is involved; and (b) to determine how the mutation relates to the region identified in the previous point. For this purpose, we have analysed for G122R:

i- Displacements of secondary structure elements or conformational changes,

ii- changes in the flexibility of residues analysing B'-factors,

iii- loss or formation of hydrogen bonding or salt bridge interactions,

iv- whether the location where these changes are observed is consistent with previously described biochemical effects.

2. Materials and methods

2.1 Chemicals

Human Triosephosphate isomerase (hTPI, GenBank number BC015100) cDNA clone was from Open Biosystems, DTT was from Promega, *Escherichia coli* strain Rosetta (DE3) and vector pET15b were from Novagen, and Phosphoglycolic acid (2-PG) was from Santa Cruz Biotechnology.

2.2 Human TPI mutagenesis, expression and purification

The cDNA of human TPI subcloned into the expression vector pET15b, downstream of the His_6-tag, was used as template to generate the G122R mutant by site-directed mutagenesis utilizing the QuikChange site-directed mutagenesis kit (Stratagene, La Jolla, CA, USA). The plasmid harboring His_6-G122R cDNA was transformed into *Escherichia coli* strain Rosetta (DE3). Cells were grown at 37°C in 1L LB medium containing ampicillin until an absorbance value of 0.8-1.0. At that time, they were induced with 0.15 mM Isopropyl β-D-thiogalactopyranoside overnight at 18°C. The cells were centrifuged,

resuspended in 20 mM Tris-HCl pH 7.5 containing 0.5 M NaCl and 10mM imidazole (column buffer), and homogenized using an EmulsiFlex-C3 device (Avestin, Inc., Ottawa, Canada). The clarified lysate was passed through a HisTrap FF column (1 mL) and it was then washed to give base-line UV absorbance with column buffer. The proteins were eluted with an imidazole gradient (0–250 mM) and the fractions containing the protein were pooled, incubated with 10 mM DTT for 2h at room temperature, desalted with 50 mM HEPES pH 7.7, 1 mM EDTA and concentrated. Protein concentrations were measured at 280 nm using the 33460 M^{-1} cm^{-1} molar extinction coefficient.

2.3 Crystallization, data collection and structure determination

8 mg/mL of apo-G122R was crystallized in 0.1 M HEPES pH 7.5, 20 % PEG 4000, and 10 % 2-propanol as previously described [1]. The crystals were grown using the hanging drop vapor diffusion method at 10 ºC. Holo-G122R was soaked for 5 minutes with 1 µL of 100mM 2-PG. The crystals were cryo-protected by soaking in a solution containing 70 % mother liquor and 30 % glycerol before being flash-frozen. Diffraction data were collected at the Protein Crystallography Beamline W01B-MX2 of the Laboratório Nacional de Luz Síncrotron (LNLS), Campinas, Brazil (wavelength = 1.4586 Å), at 100 K using a PILATUS 2M detector (Dectris). The data were processed and scaled using MOSFLM [14] and Scala [15], and subsequent analysis was performed using the CCP4 suite [16]. Both apo-G122R and holo-G122R crystals were isomorphous with the wild type human TPI crystal (PDB ID 2JK2) [9] which was used as a starting model for the refinement of the data, using the program REFMAC5 [17] after removing solvent molecules. After the proper side chains had been introduced, the models were subjected to alternating cycles of refinement in REFMAC5 and manual inspection and model building with the program COOT [18]. Ligand and solvent molecules were added to the models in the final stages of refinement based on examination of difference density maps. The atomic coordinates and structure factors (code 7UXB and 7UXV) has been deposited in Protein Data Bank (PDB) (Table 1). The structure figures were generated with PyMol program.

2.4 Structure analysis

The Baverage program (part of CCP4 suite) [19] was used to obtain a table of average B-factors and rms deviations of the main chain, the side chain of each residue and of the overall structure. The normalized B-factor (B'-factor) is equal to:

B'-factor = [B-factor$_{(main\text{-}chain\ or\ side\text{-}chain)}$ − Average B-factor$_{(main\text{-}chains\ or\ side\text{-}chains)}$]/Average rms B-factor$_{(main\text{-}chains\ or\ side\text{-}chains)}$.

The distances were determined using COOT program [18]. DelPhiForce webserver [20,21] was used to calculate the electrostatic forces.

2.5 Statistical analysis

Results were analyzed for statistical significance with the t-test (Unpaired t test or Mann-Whitney test) utilizing GraphPad Prism 5.0 software.

3. Results

3.1 G122R structure

Apo-G122R and holo-G122R crystals diffracted at 2.00 Å and 2.15 Å, respectively (Table 1). hTPI-wt structure (apo-wt, PDB ID 6UP1 and holo-wt, 6UP5) [10], were used as a control. In the four protomers of apo- and holo-G122R, the electron density around residue 122 was greater than that expected for a glycine and was attributed to arginine with the same rotameric state for all subunits (Fig. 2). The mutation did not induce conformational changes, as the root mean square deviation (rmsd) between wt and G122R did not show significant differences (data not shown), which may be due to the bulky side chain of R122 being oriented towards the solvent (Fig. 3). Regarding holo-G122R, no differences were found between wt and F240L when the contacts between 2-PG and catalytic residues were analysed (data not shown).

Table 1

Data collection and refinement statistics

Data set	apo-G122R (PDB ID 7UXB)	holo-G122R (PDB ID 7UXV)
Space group	$P2_12_12_1$	$P2_12_12_1$
a (Å)	65.20	65.12
b (Å)	75.23	75.25
c (Å)	93.20	92.80
Resolution Range (Å)	65.20-2.00 (2.05-2.00)	65.12-2.15 (2.22-2.15)
Observed reflections	177,531	139,858
Independent reflections	31,672	25,450

Rmerge (%)[a]	6.7 (23.1)	9.5 (49.2)
I/σ	14.8 (5.1)	11.5 (3.4)
Completeness (%)	99.9 (99.4)	100.0 (100.0)
Multiplicity	5.6 (4.9)	5.5 (5.7)
Refinement		
Reflections in refinement	30,092	24,120
$R_{cryst.}$ (%)[b]	17.11	18.83
R_{free}(%) (test set 5%)[c]	22.83	24.60
Average B-factor		
Protein	24.65	30.64
Ligand	34.61	47.00
Solvent	32.30	33.55
r.m.s.d. on bond lengths (Å)[d]	0.011	0.007
r.m.s.d. on bond angles (°)[d]	1.415	1.193

The values in parentheses refer to the highest resolution shells.
[a]Rmerge = Σ*h*Σ*i* | I*ih* – <I*h*> | / Σ*h*Σ*i*<I*h*>, where <I*h*> is the mean intensity of the *i* observations of reflection *h*.
[b]Rcryst = Σ | |Fobs| - |Fcalc| | / Σ |Fobs|, where |Fobs| and |Fcalc| are the observed and calculated structure factor amplitudes, respectively. The summation includes all reflections used in the refinement.
[c]Rfree = Σ | |Fobs| - |Fcalc| | / Σ |Fobs|, evaluated for a randomly chosen subset of 5% of the diffraction data not included in the refinement.
[d] Root mean square deviation from ideal values.

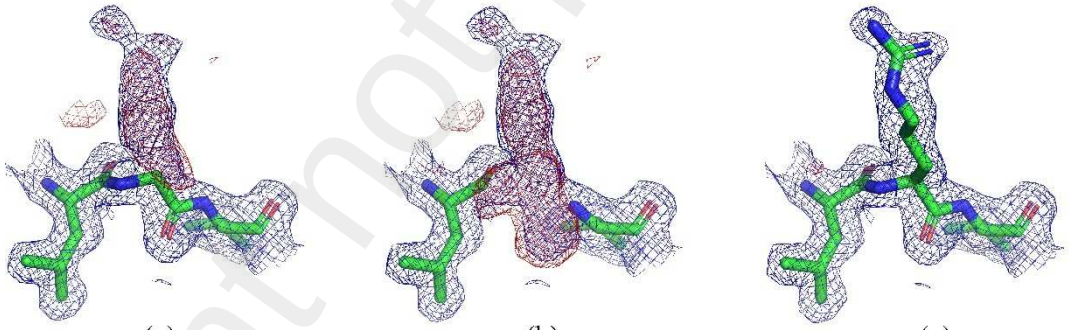

Figure 2. Electron density map showing the mutation of glycine to arginine at position 122 of the apo-G122R structure (d = 2.00Å). 2Fo-Fc (in blue) and Fo-Fc (in red) density maps contoured at 1σ and 3σ, respectively, were generated around residue 122 when it was modelled as (a) glycine or (c) as arginine. (b). The omit map was generated by omitting residue G122.

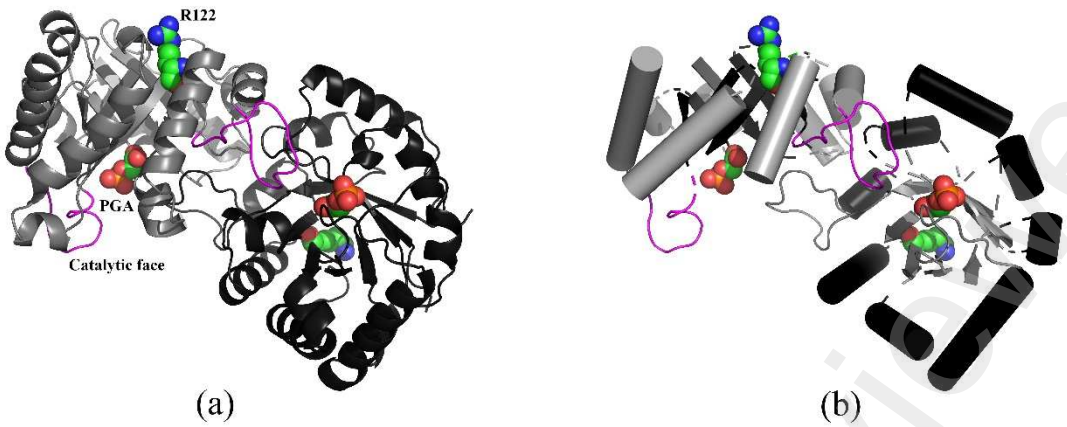

Figure 3. R122 localisation. (a). Structure of holo-G122R (grey, A subunit; dark grey, B subunit). (b). The secondary structure elements of holo-wt belonging only to the (β/α) 8-barrel fold. The R122 residue (in green) and 2-PG (in orange) are shown as spheres.

3.2 Flexibility of residues: analysing the B'-factors

The analysis of the increase in flexibility in the G122R structure was the approach used to identify the region affected by the mutation. To do this, normalised values of the B-factor (B'-factor) of the main or side chains were obtained from the PDB files and compared between wt and G122R (see Materials and methods). The B'-factor is used as a tool to identify flexibility in different parts of the protein structure [22]. High values of the B'-factor indicate high flexibility or mobility, whereas low values indicate more rigid positions. The B'-factor values of each residue of wt or G122R were taken from four protomers (two from apo- and two from holo-wt/G122R), so n=4 is available for statistical analysis. This provides strong statistical support for the changes in the B' factor between wt and G122R, making the results reliable. However, for a correct analysis of changes in B'-factor values, certain typical structural features of TPI-wt must be taken into account:

A) The catalytic loop (residues 167–177) is known to show high mobility in several TPI structures. Here, the catalytic loop of the apo-B subunit and holo-G122R show high mobility, which is reflected in their high B'-factors. The loop interacts with α7 and α8, and these regions also show high mobility [10]. Thus, it is not possible to reliably analyse changes in mobility between the wt and G122R with residues involved in those secondary elements.

B) The holo-structures were obtained by 5 min of crystal soaking with 2-PG, and therefore, the residues that interact with it at the catalytic site have high B'-factor values compared to the apo-structures. Thus, as catalytic loop residues, it is not possible to reliably analyse changes in the mobility of these residues between the wt and G122R.

However, it is important to note that residue 122 is not affected by the mobile parts mentioned above, as it is located on the noncatalytic face, at the N-terminus of β6 (Fig. 1d and Fig. 3). Therefore, in order to analyse and identify the residues affected by the mutation, the B'-factors of each residue belonging to all the α-loop-β segments of the noncatalytic face (Fig. 1d) of the (β/α) 8-barrel were determined. We are certain that a residue is affected by the mutation when its B'-factor value in G122R is significantly higher than in wt. The highest values of the B'-factors correspond to less negative values indicated on the inverted ordinate axis in Fig. 4 and Fig. S1. Fig. 4 shows the segments α-loop-β, where the residues that have increased B'-factors on the main chain or side chain have been found. The rest can be seen in Fig. S1. Residues K18, L24, I25, G26 and N29, all belonging to α1, were found to be affected in the main chains and/or in the side chains (Fig. 4a and b), together with D49, R52, Q53, K54, L55 and A60, belonging to α2, L2 and β3 (Fig. 4c and d). On the other hand, residues V143, T147, V149, A151, D156, E183, V184 were found with a decrease in B'-factors (Fig. S1). These residues belong to α7 and α8. As mentioned above, these α-helixes interact with the catalytic loop and were not analysed.

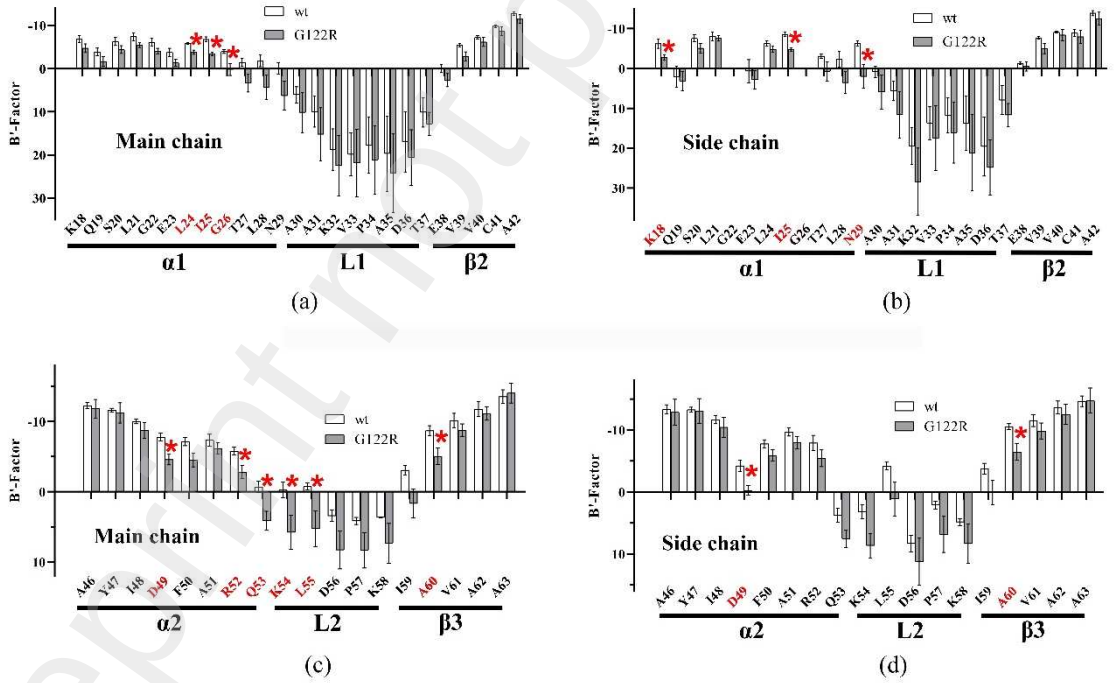

Figure 4. Flexibility analysis of residues located in the noncatalytic face. B′-factors of the main chain (a, c) or side chain (b, d) for each residue (belonging to segment α1-L1-β2 or α2-L2-β3) corresponding to the A and B subunits of each apo-structure and holo-structure (n = 4). The highest values of the B′-factors correspond to less negative values indicated on the ordinate axis. Values represent mean ± SEM. * Significantly different ($P < 0.05$).

3.3 Non covalent interactions of R122

LIGPLOT software was used to identify all residues that form hydrogen bonds or salt bridges with the side chain of R122. This was done to correlate the effect of the presence of a positively charged amino acid, such as R122, with the increased mobility of the residues shown in Fig. 4. This analysis was performed on four G122R subunits (two from apo-G122R and two from holo-G122R). It was found that the side chain of R122 only forms a hydrogen bond with E38 through a water molecule (Fig. 5) and does not form a salt bridge with other residues. However, E38 showed no increase in B'-factor (Fig. 4a and b), probably because its side chain forms a salt bridge with R205 and two hydrogen bonds with W90 and R205 (data not shown). As will be mentioned later, the more hydrogen bonds a residue has on the side chain, the more stable its position will be and therefore it will have a lower B'-Factor value, which means it will have less mobility. Under these conditions, an increase in mobility due to the appearance of a charged residue such as R122 is less likely.

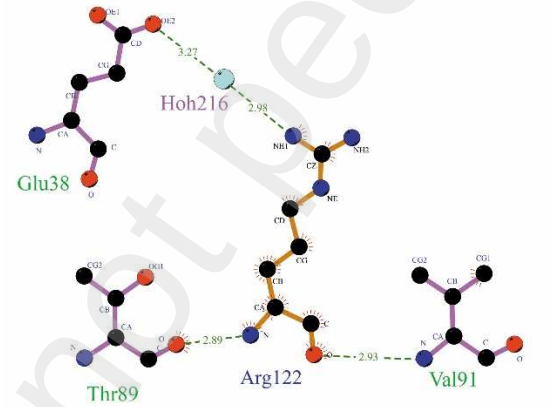

Figure 5. Schematic diagram of hydrogen bond network linked to R122 (represented by dashed lines) generated by LIGPLOT software using holo-G122R PDB files. Water molecules are indicated as "hoh".

3.4 Long-range electrostatic interaction of R122

Since the presence of R122 did not induce conformational changes or salt bridge formation, and its single hydrogen bond interaction with E38 through a water molecule had no effect, then the possibility that the effect was a consequence of a long-range electrostatic interaction was evaluated. Long-range electrostatic interactions are known to be important in catalysis [23], protein stability [24], protein interaction [25], etc. Coulombic interactions between charged residues separated by 15 Å or 26 Å have been described to play a key role in transition state complex stability in catalysis [23] or in protein binding [25]. For these analyses, charged residues that are affected only at their

side chains (where the charge is located) have been selected from Fig. 4b and d. There, K18 and D49 are the only charged ones affected in the side chains. While the shortest distance between R122 and D49 is with both residues in the same subunit (20.10 ± 0.08 Å), the shortest distance between R122 and K18 is with each residue in a different subunit (20.48 ± 0.19 Å). In order to understand why K18 and D49, but not other charged residues closer to R122, were affected, all charged residues located on the noncatalytic face and up to a distance of 25 Å from R122 (Fig. 6) were analysed, comparing the B'-factor of the side chains and counting the number the hydrogen bonds established in the side chain by each charged residue in order to determine the degree of stabilisation that would compensate for the long-range electrostatic influence of the presence of R122. The number the hydrogen bonds was determined using LIGPLOT software and both, apo- and holo-structures of wt and G122R.

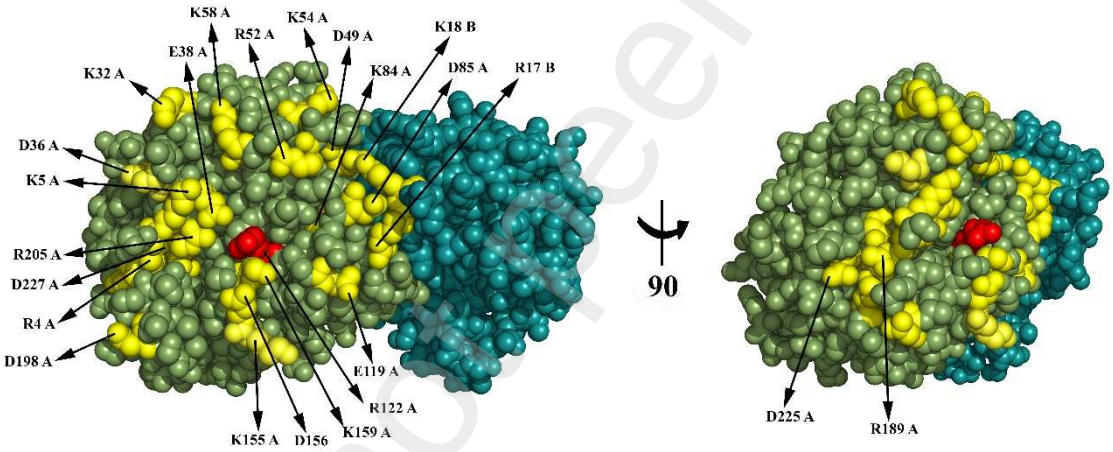

Figure 6. Charged residues on the noncatalytic face. The A and B subunits of apo-G122R are shown in green and blue respectively. R122 are shown in red and the charged residues included in Figure 4 are shown in yellow.

The B'-factors of charged residues ordered by distance from R122 are shown in Fig. 7a and by number of hydrogen bonds established with other residues in Fig. 7b. It is clear that there is a strong correlation between the values of the B'-factors and the number of hydrogen bonds, the interpretation being that the lower stabilization leads to higher mobility. (Fig. 7 b).

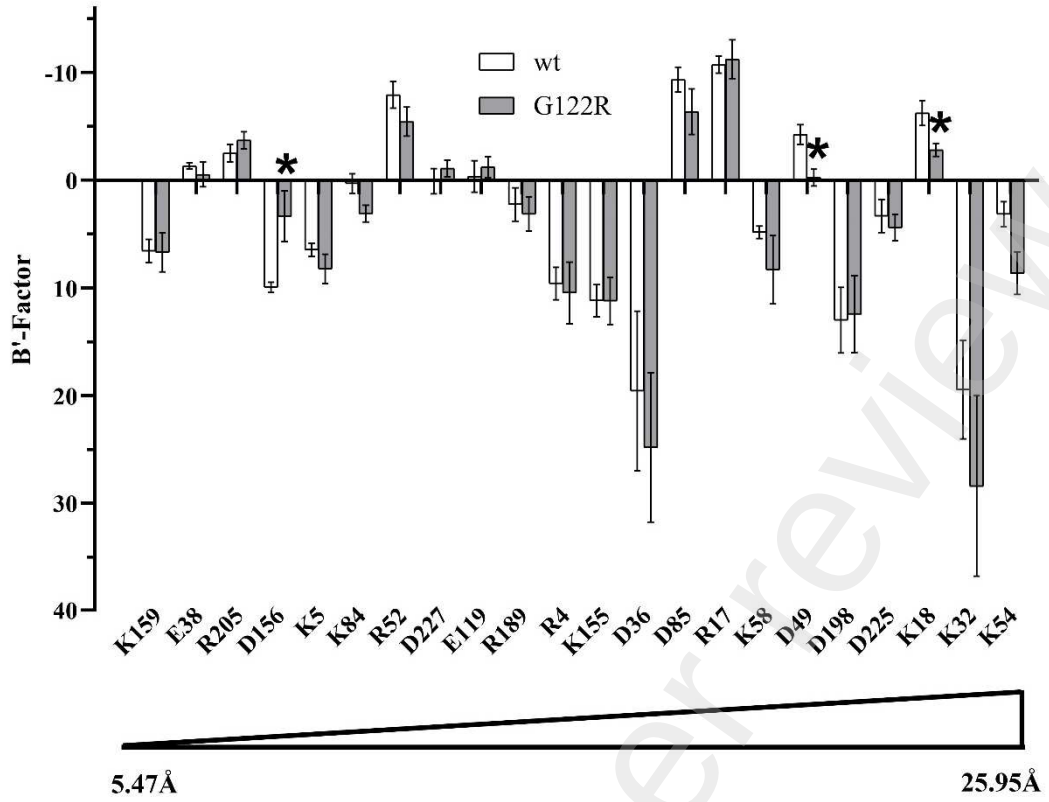

(a)

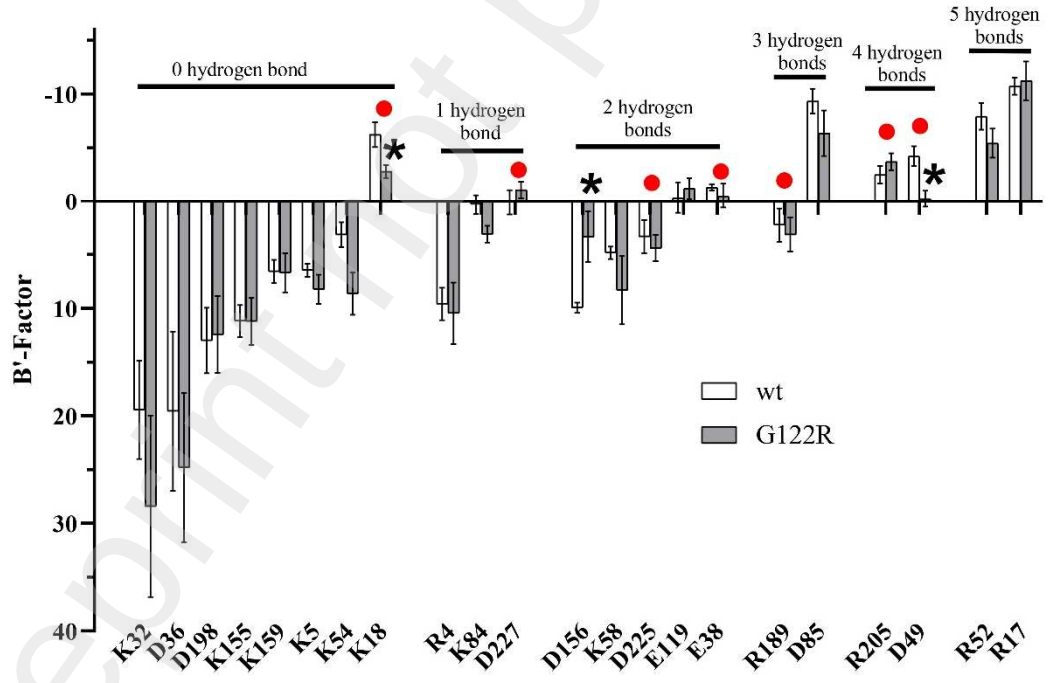

(b)

Figure 7. Flexibility analysis of charged residues located in the noncatalytic face. B′ factors of the side chain for each residue corresponding to residues of the A and B subunits of each apo structure and holo structure, (n = 4). (a). Charged residues arranged according to distance form R122. (b). Charged residues

arranged according to the number of hydrogen bonds on their side chains (for wt and G122). Red filled circles identify residues that form salt bridges. The highest values of the B′ factors correspond to less negative values indicated on the ordinate axis. Values represent mean ± SEM. * Significantly different ($P < 0.05$).

With the exception of D156 and D49, the 17 residues shown in Fig. 7a that are at a shorter distance from R122 than K18 not showed difference in the B'-factors between wt and G122R, and therefore were not affected by the mutation, since they showed either high mobility or high stabilisation. K159, K5, K155, D36 and D198 have no hydrogen bonds and therefore they have exhibit high mobility. R4, K84 and D227 have one hydrogen bond but still have some mobility. The same applies to K58, D225, E199 and E38, although they have two hydrogen bonds. The remaining residues have more than three hydrogen bonds and therefore show high stability (low mobility). Thus, K18 is unique compared to the other 17 residues. In wt, it has no hydrogen bonds and is therefore not stabilised and yet has low mobility. This structural feature explains why K18 could be the target of effect of the mutation. With regard to D156, a lower value of the B'-factor was observed in the mutant. This is due to the fact that D156 forms an additional hydrogen bond with K159 in G122R, since the side chain of K159 (close to R122) changes its orientation in the presence of R122 and approaches D156. (Fig. 8). This change in orientation reduces the distance between the carbonyl O atom of D156 and the amine N atom of K159 from 3.64 ± 0.02 Å in wt to 3.21 ± 0.04 Å in G122R (Significantly different, $P < 0.05$). Regarding charged side chains, the distance between the $O^{\delta 2}$ atom of D156 and the N^{ζ} atom of K159 is also reduced from 7.29 ± 0.11 Å to 4.51 ± 0.18 Å (Significantly different, $P < 0.05$). As a consequence of these interactions D156 is more stable in G122R, which is why it showed a lower B´-factor value than the wt. With respect to D49, it establishes four hydrogen bonds through its side chain, stabilising it. However, the B'-factor increased. D49 forms a salt bridge with K18 (Fig. 9a, red dashed line), which is the cause of its increased mobility.

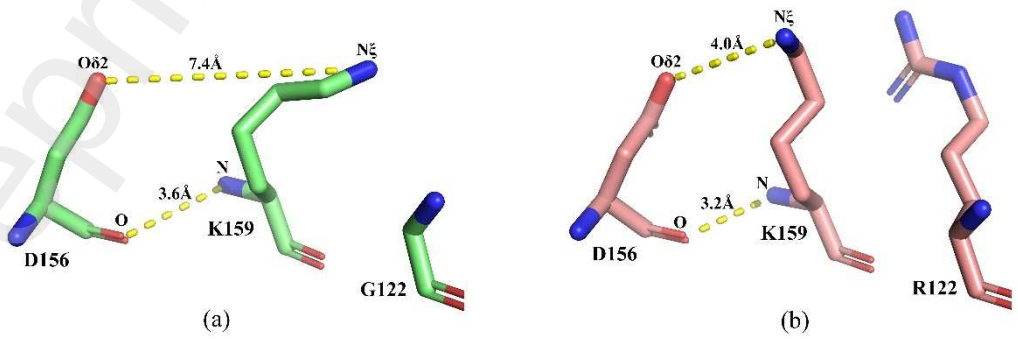

Figure 8. D156 stabilisation. (a). Position of K159 in the A subunit of apo-wt. (b). Position of K159 in the A subunit of apo-G122R. The yellow dashed line indicates the distance between the atoms.

3.5 Hydrogen bond network linked to K18 and D49

With K18 being the target of the effect of the mutation, all residues in its hydrogen bonding network could be affected. This would increase the B'-factors depending on their degree of stabilisation. Fig. 9a shows the hydrogen bond network linked to K18 and D49 in different subunits, generated by LIGPLOT software. Fig. 9a clearly demonstrates that several residues in the hydrogen bonding network are also those identified to be affected by the mutation in Fig. 4 (G26, R52, Q53 and L55). The other affected residues in Fig. 4 (L24, I25, N29, K54 and A60) are not present in the network, but the neighbouring residues in the chain are present (E23, G26, A30, L55, I59), which according to Fig. 4 have a non-statistically significant increase in the B' factor in G122R. As shown in Fig. 9b, this hydrogen bonding network is located at the dimeric interface and, as E104D and F240L, G122R also affected the dimeric interface.

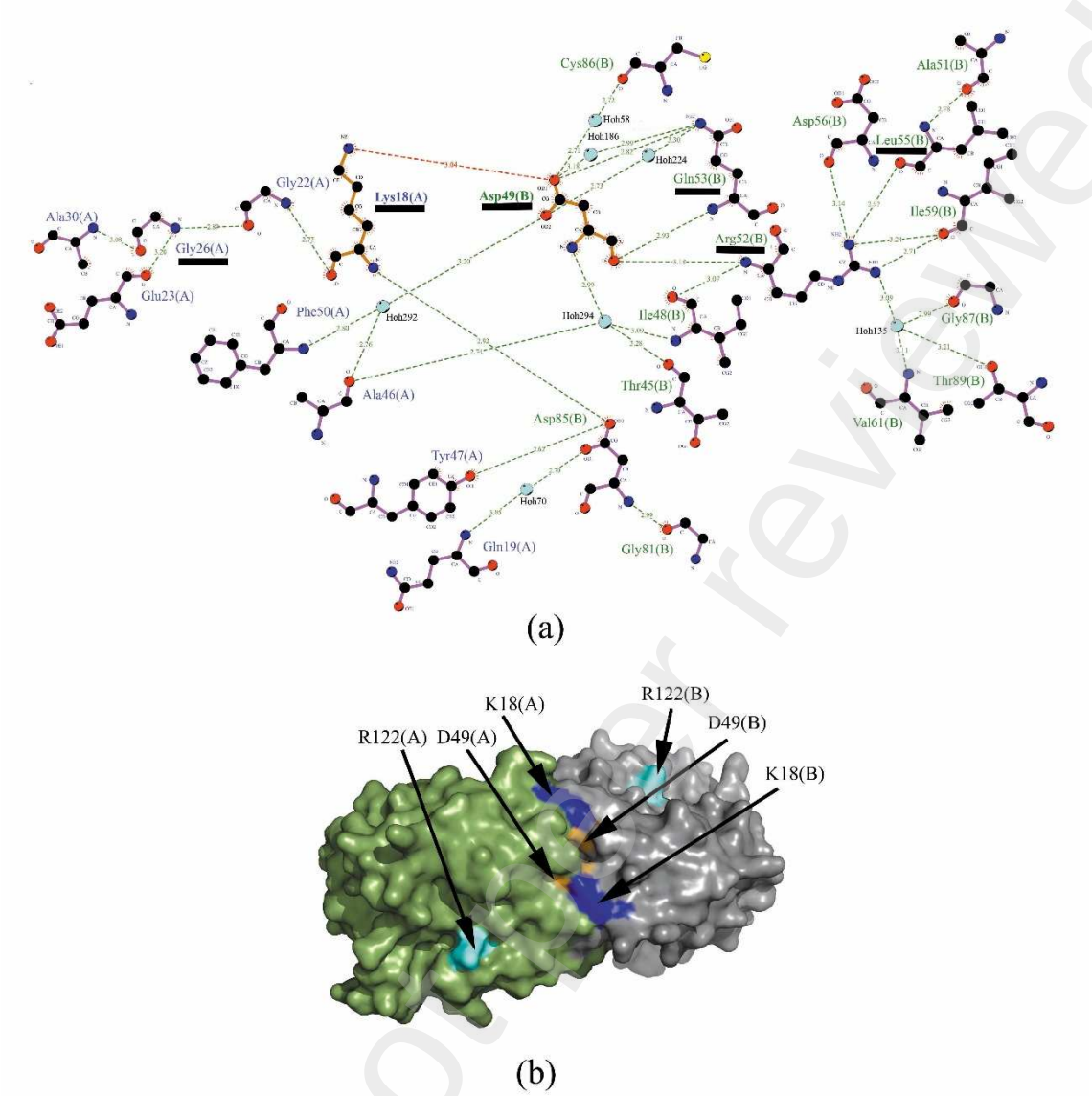

Figure 9. Location of residues affected by the mutation. (a). Schematic diagram of the hydrogen bond network linked to K18 and D49 (represented by green dashed lines) generated by LIGPLOT software using apo-G122R coordinates. Residue labels belonging to A or B subunits are coloured in blue and green, respectively. The red dashed line represents the salt bridge. Water molecules are shown as "hoh". The residues identified in Figure 4 are underlined in black. (b). Surface representation of apo-G122R, where A-subunit and B-subunit are shown in green and grey, respectively. R122, D49 and K18 are shown in cyan, orange and blue, respectively.

4. Discussion

Human triosephosphate isomerase G122R, also known as TPI-Manchester, has been described as thermolabile [11-13]. Previous structural studies using crystallographic structures have been performed with E104D and F240L [9,10]. They are also thermolabile and in both cases the mutation affected the dimer interface. Calorimetric studies carried out on the recombinant version showed that the Tm for E104D, F240L and G122R was approximately 20 %, 15 % and 5 % less than wt, respectively [26], suggesting that a large

loss of thermostability is not necessary to induce disease. Here we solved the crystal structure of apo-G122R and holo-G122R and used these coordinates to analyse which region of the structure is affected by the mutation and how the mutation relates to it. As shown in Fig. 4, residues belonging to α1 and L2, which are both involved in the dimer interface, were affected by the mutation (Fig. 4 and Fig. 9). However, R122 is located approximately 20 Å from the dimer interface. In an attempt to link R122 to these residues, LIGPLOT software was used to identify the hydrogen bonding network associated with the side chain of R122. Only E38 was found to form a hydrogen bond with R122 side chain, however E38 was not affected according to its B´-factors value (Fig. 4). Thus, the connections of R122 with the affected zone through short-range interactions such as hydrogen bonds or salt bridges were not found. Therefore, long-range electrostatic interactions were evaluated. For this, the charged residues of the affected zone and all charged residues up to 25 Å of R122 were analysed (Fig. 6 and Fig. 7). In the wt, only K18 showed a peculiarity: it has no hydrogen bond on its side chain and would therefore be poorly stabilised and yet showed a low B'-factor. Probably the salt bridge with D49 is responsible for the low B'-factor. This rigidity, with little stabilisation, would be easily modified by the appearance of a charge such as R122. The rest of the charged residues showed either high mobility or high stabilisation. Here, high mobility (higher B'-factor values) correlates with the absence or low amount of hydrogen bonding in the side chains. Because of this high mobility, the effect of an increase in its mobility as a result of the appearance of a charge such as R122 could not affect its already high B'-factor value. On the other hand, low mobility correlates with a large number of hydrogen bonds and therefore the side chain position will be more stable (low B'-factors). As mentioned above for E38, under these conditions an increase in mobility due to the appearance of a charged residue is less likely. Long-range electrostatic interactions have been implicated in stabilisation, binding, catalysis, etc. [23-25]. It is not clear how large the distance between the charges can be for the interaction to be effective. For example, Jackson S. E. et al. found a stabilising role for D36 and D99 on the transition state complex of the serine protease subtilisin BPN. Both were located 15.2 Å and 12.6 Å from the complex, respectively [23]. Pabbathi A. et al. identified D3402 and E3320 as modulators of the affinity between dynein and microtubule binding, located at 26 Å and 12 Å from the binding interface, respectively [25]. The electrostatic force between R122 and K18 was calculated using the DelPhiForce webserver [20,21]. It was found to be 0.086 ± 0.003 kT/Å. This value is in agreement with other long-range electrostatic calculations

performed in the interaction between α/β tubulin [27] and kinesin-5 and tubulin [28]. To validate the effect of a mutation, alternative mutations are often generated. Crystallising G122K and analysing whether K122 has the same effect as R122 could be one possibility. However, although both arginine and lysine are positively charged residues, they differ in length and charge distribution. Therefore, the effect may or may not be replicated. On the other hand, it could be considered as sufficient information to validate the results to have four structures (n=4) to analyse the effects. As a method of supporting studies of flexibility or residue movement in proteins, molecular dynamics is often used. However, we can observe mobility without recourse to simulation by using PDB files to calculate B' factors. In conclusion, the present study is an analysis of the structural effects of the TPI-Manchester mutant. This work is intended to complete the studies initiated by Dr H.W. Mohrenweiser a pioneer in the study of this hTPI mutant.

Funding

This work was supported by grants from Consejo Nacional de Investigaciones Científicas y Técnicas (CONICET), Fondo para la Investigación Científica y Tecnológica (FONCyT) and Secretaría de Ciencia y Técnica-Universidad Nacional de Córdoba (SECyT-UNC).

Acknowledgments

I wish to thank Dr. María Elena Carrizo for her help in processing the crystal diffraction datasets and for critical review of the manuscript. This research used resources of the Brazilian Synchrotron Light Laboratory (LNLS), an open national facility operated by the Brazilian Centre for Research in Energy and Materials (CNPEM) for the Brazilian Ministry for Science, Technology, Innovations and Communications (MCTIC). The W01B-MX2 beamline staff is acknowledged for the assistance during the experiments.

References

[1] D.W. Banner, A.C. Bloomer, G.A. Petsko, D.C. Phillips, C.I. Pogson, I.A. Wilson, P.H. Corran, A.J. Furth, J.D. Milman, R.E. Offord, J.D. Priddle, S.G. Waley, Structure of chicken muscle triose phosphate isomerase determined crystallographically at 2.5 angstrom resolution using amino acid sequence data, Nature 255 (1975) 609-614.

[2] R. Sterner, B. Höcker, Catalytic versatility, stability, and evolution of the (beta-alpha) 8-barrel enzyme fold, Chem. Rev. 105 (2005) 4038-4055.

[3] N.S. Sampson, J.R. Knowles, Segmental movement: definition of the structural requirements for loop closure in catalysis by triosephosphate isomerase, Biochemistry 31 (1992) 8482–8487.

[4] A.S. Schneider, Triosephosphate isomerase deficiency: historical perspectives and molecular aspects, Baillieres Best Pract. Res. Clin. Haematol. 13 (2000) 119-140.

[5] F. Orosz, J. Oláh, J. Ovádi, Triosephosphate isomerase deficiency: facts and doubts, IUBMB Life 58 (2006) 703-715.

[6] M. Ralser, G. Heeren, M. Breitenbach, H. Lehrach, S. Krobitsch, Triosephosphate isomerase deficiency is caused by altered dimerization not catalytic inactivity of the mutant enzymes, PLoS One 20 (2006), 30.

[7] F. Orosz, J. Oláh, J. Ovádi, Triosephosphate isomerase deficiency: new insights into an enigmatic disease, Biochim. Biophys. Acta 1792 (2009) 1168-1174.

[8] B.P. Roland, K.R. Richards, S.L. Hrizo, S. Eicher, Z.J. Barile, T.C. Chang, G. Savon, P. Bianchi, E. Fermo, B.M. Ricerca, L. Tortorolo, J. Vockley, A.P. VanDemark, M.J. Palladino, Missense variant in TPI1 (Arg189Gln) causes neurologic deficits through structural changes in the triosephosphate isomerase catalytic site and reduced enzyme levels in vivo, Biochim. Biophys. Acta (BBA), Mol. Basis Dis. 1865 (2019) 2257-2266.

[9] C. Rodríguez-Almazán, R. Arreola, D. Rodríguez-Larrea, B. Aguirre-López, M.T. de Gómez-Puyou, R. Pérez-Montfort, M. Costas, A. Gómez-Puyou, A. Torres-Larios, Structural basis of human triosephosphate isomerase deficiency: mutation E104D is related to alterations of a conserved water network at the dimer interface, J. Biol. Chem. 283 (2008) 23254-23263.

[10] J.M. Romero, Triosephosphate isomerase deficiency: Effect of F240L mutation on enzyme structure, Archives of Biochemistry and Biophysics 689 (2020) 108473.

[11] R.S. Decker, H.W. Mohrenweiser, Origin of the Triosephosphate Isomerase Isozymes in Humans: Genetic Evidence for the Expression of a Single Structural Locus, Am. J. Hum. Genet. 33 (1981) 683-691.

[12] J. Asakawa, H.W. Mohrenweiser, Characterization of Two New Electrophoretic Variants of Human Triosephosphate Isomerase: Stability, Kinetic, and Immunological Properties, Biochemical Genetics 20 (1982) 59-76.

[13] B.A. Perry, H.W. Mohrenweiser, Human triosephosphate isomerase: substitution of Arg for Gly at position 122 in a thermolabile electromorph variant, TPI-Manchester, Hum. Genet. 88 (1992) 634-638.

[14] A.G.W. Leslie, Recent changes to the MOSFLM package for processing film and image plate data Jnt. CCP4/ESF-EACMB, Newslett. Protein Crystallogr. 26 (1992) 27-33.

[15] P.R. Evans, Scaling and assessment of data quality, Acta Crystallogr. D. Biol. Crystallogr. 62 (2006) 72-82.

[16] M.D. Winn, C.C. Ballard, K.D. Cowtan, E.J. Dodson, P. Emsley, P.R. Evans, R.M. Keegan, E.B. Krissinel, A.G. Leslie, A. McCoy, Overview of the CCP4 suite and current developments, Acta Crystallogr. D. Biol. Crystallogr. 67 (2011) 235-242.

[17] G.N. Murshudov, A.A. Vagin, E.J. Dodson, Refinement of macromolecular structures by the maximum-likelihood method, Acta Crystallogr. D. Biol. Crystallogr. 53 (1997) 240-255.

[18] P. Emsley, B. Lohkamp, W.G. Scott, K. Cowtan, Features and development of coot, Acta Crystallogr. D Biol. Crystallogr. 66 (2010) 486-501.

[19] M.D. Winn, C.C. Ballard, K.D. Cowtan, E.J. Dodson, P. Emsley, P.R. Evans, R.M. Keegan, E.B. Krissinel, A.G. Leslie, A. McCoy, S.J. McNicholas, G.N. Murshudov, N.S. Pannu, E.A. Potterton, H.R. Powell, R.J. Read, A. Vagin, K.S. Wilson, Overview of the

CCP4 suite and current developments, Acta Crystallogr D. Biol Crystallogr. 67 (2011) 235-242.

[20] S. Sarkar, S. Witham, J. Zhang, M. Zhenirovskyy, W. Rocchia, E. Alexov, DelPhi Web Server: A comprehensive online suite for electrostatic calculations of biological macromolecules and their complexes, Comm. Comp. Phys. 13 (2013) 269-284.

[21] L. Li, Z. Jia, Y. Peng, A. Chakravorty, L. Sun, E. Alexov, DelPhiForce web server: electrostatic forces and energy calculations and visualization, Bioinformatics 15 (2017) 3661-3663.

[22] Z. Sun, Q. Liu, G. Qu, Y. Feng, M.T. Reetz, Utility of B-factors in protein science: interpreting rigidity, flexibility, and internal motion and engineering thermostability, Chem. Rev. 119 (2019) 1626-1665.

[23] S.E. Jackson, A.R. Fersht, Contribution of long-range electrostatic interactions to the stabilization of the catalytic transition state of the serine protease subtilisin BPN', Biochemistry 32 (1993) 13909-13916.

[24] G.R. Grimsley, K.L. Shaw, L.R. Fee, R.W. Alston, B.M.P. Huyghues-Despointes, R.L. Thurlkill, J.M. Scholtz, C.N. Pace, Increasing protein stability by altering long-range coulombic interactions, Protein Science 8 (1999)1843–1849.

[25] A. Pabbathi, L. Coleman, S. Godar, A. Paul, A. Garlapati, M. Spencer, J. Eller, J.D. Alper, Long-range electrostatic interactions significantly modulate the affinity of dynein for microtubules, Biophysical Journal, 121 (2022) 1715–1726.

[26] N. Cabrera, A. Torres-Larios, I. García-Torres, S. Enríquez-Flores, R. Perez-Montfort, Differential effects on enzyme stability and kinetic parameters of mutants related to human triosephosphate isomerase deficiency, Biochim. Biophys. Acta 1862 (2018) 1401-1409.

[27] W. Guo, T.A. Ale, S. Sun, J.E. Sanchez, L. Li, A Comprehensive Study on the Electrostatic Properties of Tubulin-Tubulin Complexes in Microtubules, Cells 12 (2023) 238.

[28] W. Guo, S. Sun, J.E. Sanchez, A.E. Lopez-Hernandez, T.A. Ale, J. Chen, T. Afrin, W. Qiu, Y. Xie, L. Li, Using a comprehensive approach to investigate the interaction between Kinesin-5/Eg5 and the microtubule, Comput. Struct. Biotechnol. J. 20 (2022) 4305–4314.